Stability and Elasticity of Quasi-Hexagonal Fullerene Monolayer from First-Principles Study

Guichang Shen [1], Linxian Li [1], Shuai Tang [1,*], Jianfeng Jin [2], Xiao-Jia Chen [3] and Qing Peng [3,4,5,*]

1   State Key Laboratory of Rolling and Automation, Northeastern University, Shenyang 110819, China
2   School of Materials Science and Engineering, Northeastern University, Shenyang 110819, China
3   School of Science, Harbin Institute of Technology, Shenzhen 518055, China
4   State Key Laboratory of Nonlinear Mechanics, Institute of Mechanics, Chinese Academy of Sciences, Beijing 100190, China
5   School of Engineering Sciences, University of Chinese Academy of Sciences, Beijing 100049, China
*   Correspondence: tangshuai@ral.neu.edu.cn (S.T.); pengqing@imech.ac.cn (Q.P.)

Abstract: As a newly synthesized two-dimensional carbon material, the stability study of monolayer fullerene networks or quasi-hexagonal phase fullerenes (qhp-C_{60}) is timely desirable. We have investigated the stabilities of qhp-C_{60}, including thermal, structural, mechanical, and thermodynamic stabilities, as well as the bonding characteristics, ductility, and mechanical properties, via first-principles calculations. The results show that qhp-C_{60} is energetically, mechanically, and thermodynamically stable. The thermodynamic stability of qhp-C_{60} at 300 K and 600 K is verified. The bonding characteristics of qhp-C_{60} are analyzed from the bond length, and it has sp^2 and sp^3 hybridization. The Pugh ratio (B/G) and Poisson's ratio (v) indicate similar ductility with graphite and graphene. We also found that qhp-C_{60} has the lowest hardness and the anisotropy of the material. In addition, the electronic characteristics, including electron localization function (ELF), crystal orbital Hamiltonian population (COHP), and density of states (DOS) at different temperatures, are analyzed to verify the thermal stability of the material. Our results might be helpful in the material design of qhp-C_{60}-related applications.

Keywords: qhp-C_{60}; stability; first-principles; mechanical properties

1. Introduction

Carbon-based two-dimensional (2D) materials have attracted extensive attention because of their unique and rich properties, functions, and applications. As the paradigm of 2D materials, graphene has a perfect sp^2 hybridized carbon structure in a two-dimensional plane. In addition, it has excellent electronic, thermal, optical, and mechanical properties [1–3]. Graphene has been successfully used to fabricate field-effect transistors (FETs) [4–6], transparent conducting electrodes [7–9], supercapacitors [10,11], and lithium-ion batteries [12]. The successful preparation of graphene [13] has shown that it is possible to exfoliate stable, single-atom, or single-polyhedral-thick 2D materials from van der Waals solids. These materials can exhibit unique and fascinating physical properties. Frindt et al. showed that layered van der Waals materials, such as layered metal dichalcogenides, could be mechanically and chemically exfoliated into few and single layers [14,15]. Novoselov et al. isolated individual monolayers from various layered materials, including *h*-BN and dihydroxides (e.g., MoS_2 and $NbSe_2$) [16]. Moreover, fullerenes have interesting electronic and magnetic properties. Superconductivity was also found in fullerene compounds [17–20]. Thus, scientists want to prepare 2D fullerene, further studying its intrinsic properties. Hou et al. prepared a large-size monocrystalline 2D carbon material, a monolayer of quasi-hexagonal crystalline phase fullerene (C_{60}), by interlayer bonding cleavage [21]. This 2D material has good thermodynamic stability and high crystallinity. In

particular, this monolayer polymer C_{60} has a moderate band gap of about 1.6 eV, solving the problem of zero band gap in graphene.

In practical applications, the stability of materials is an essential factor affecting the reliability and lifetime of devices. The structure and properties of 2D materials are susceptible to environmental conditions [22–28], so the stability of 2D materials is critical. With the development of computer science, first-principles calculation has shown great advantages in the stability of materials. So far, several studies on the stability of carbon materials have been carried out. Sen et al. studied the thermal stability of sp^3-bonded 2D carbon allotropes using ab initio molecular dynamics [29]. This study shows that only low-energy structures can be stable under environmental conditions. Li et al. reported that monolayer *h*-BN shows strong thermal stability when heated in the air [30]. Wen et al. investigated the mechanical stability of simple cubic carbon [31]. Simple cubic carbon is mechanically stable above 400 GPa. And an excellent mechanical and thermodynamic stability of carbon can be found above 2700 GPa. Lu et al. discovered that metastable carbon allotrope could withstand temperatures up to 1000 K by first-principles study, and its in-plane stiffness is greater than that of graphene [32]. He et al. found that both sp^2-diamond and cubic-graphite are dynamically stable by phonon spectroscopy. The band gap of sp^2-diamond is 1.66 eV, and it is a semiconductor [33]. Luo et al. found that biphenylene is dynamically stable and has a melting point of up to 4500 K by first-principles calculation [34]. Mortazavi et al. showed that the qhp-C_{60} has desirable dynamical stability through predicted phonon dispersion [35]. However, they explored the unilateral stability of qhp-C_{60} only. There is still a lack of systematic research into the stability of qhp-C_{60}. In addition, the analysis of the electronic structure is effective for obtaining the interactions between atoms and the properties of the material. Mei et al. found that octagonal-C is metallic and the C-C bond is predominantly covalent by electronic analysis [36]. Alborznia et al. showed that in the presence of applied pressure, the band gap of T-Carbon becomes smaller, but it is still a semiconductor material [37]. Wang et al. found that sp^3 hybridization facilitates the formation of a symmetrical lattice structure to ensure the high hardness of the carbon material [38]. Thus, electronic structure analysis provides insight into the potential applications of the material.

In this paper, we have assessed the stability of the qhp-C_{60} structure (structural, mechanical, and thermodynamic stability), bonding characteristics, ductility, and mechanical properties using first-principles calculations. The stability and bonding changes of the materials at different temperatures were analyzed by electron localization function (ELF) and crystal orbital Hamiltonian population (COHP). In addition, the contribution of orbitals at different temperatures is analyzed by using density of states (DOS). The result shows that quasi-hexagonal fullerene monolayer offers an interesting platform for potential application in 2D electronic devices.

2. Materials and Methods

Density functional theory (DFT) calculations are carried out using the Vienna ab initio simulation package (VASP) in the study [39]. The electron interaction with ions was replaced by the projector augmented wave (PAW) method, and exchange-correlation potentials between electrons were parameterized by the generalized gradient approximation (GGA) with Perdew–Burke–Ernzerhof (PBE) function [40,41]. The qhp-C_{60} primitive cell containing 60 carbon atoms was used. The conjugate-gradient algorithm was used to relax all atomic positions and cell size to achieve the minimum total energy of the systems until the average force on each atom is less than 0.01 eV/atom. The plane-wave cutoff energy was specified as 520 eV for all models. The $4 \times 4 \times 1$ k-points mesh obtained by the Monkhorst-Pack method was employed to sample the Brillouin zone. The total energy convergence was set to 10^{-6} eV/atom. A 15 Å (1 Å = 0.1 nm) vacuum layer was set along the z-axis direction to avoid the influence of the interaction force between atomic layers. The energy-strain relationship was used to calculate elastic constants. For the quadratic symmetry 2D materials, the orthogonal lattice transformed by selecting the $[-110]$ $[-1-10]$

[001] direction to redefine the coordinate axis was selected and the energy–strain method was used to calculate elastic constants. The structure's stability was ensured by the energy minimization during the structure relaxation via the conjugate gradient method [42]. AIMD simulations were performed to verify the thermodynamic stability of qhp-C_{60} at finite temperatures. In doing this, a $2 \times 2 \times 1$ supercell of qhp-C_{60} was simulated within the NVT systems by using the Nose–Hoover thermostat for 10 ps with a time step of 0.0001 ps at 300 K and 600 K, and a $1 \times 1 \times 1$ k-point mesh.

3. Results

3.1. Crystal Structure, Thermal, and Structural Stability

3.1.1. Crystal Structure

The crystallographic results of qhp-C_{60} are shown in Figure 1a. The structure parameters after relaxation are listed in Table 1, along with the calculated structures of other carbon materials (graphite, graphene, and diamond). The calculated values of our obtained structure parameters are in agreement with those of the references, demonstrating the accuracy of our calculations.
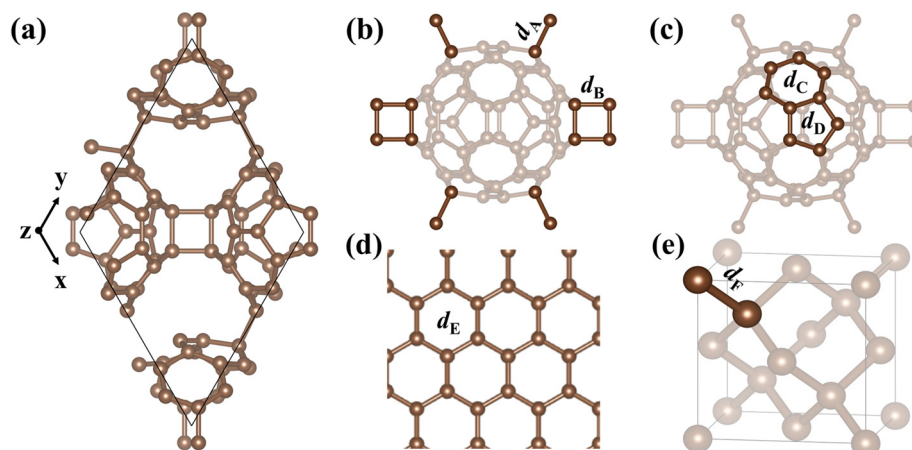

Figure 1. Crystal structure (**a**–**c**) qhp-C_{60}, (**d**) graphite, and (**e**) diamond. Here, d_A–d_D, d_E, and d_F are the bond length of qhp-C60, graphite, graphene, and diamond.

Table 1. Lattice constants (Å), bond lengths (Å), formation, and binding energies (eV/atom) of the four carbon materials.

Compound	a	b	c	Bond Lengths	ΔH	ΔE	Ref.
Graphite	2.47	2.27	6.74	1.42		−9.20	Present
	2.46	2.46	6.70	1.42			[43]
Graphene	2.47	2.47	-	1.42	0.05	−9.15	Present
	2.47	2.47	-	1.42		−9.22	[44]
Diamond	3.57	3.57	3.57	1.55	0.27	−8.93	Present
	3.57	3.57	3.57	1.55		−9.09	[45]
qhp-C_{60}	9.15	9.15	7.00	1.41–1.64	0.45	−8.75	Present

The results in Figure 1 and Table 1 show d_A = 1.64 Å, d_B = 1.61 Å, d_C = 1.41–1.45 Å, d_D = 1.44–1.45 Å, d_E = 1.42 Å, and d_F = 1.55 Å. Liu et al. showed that the length of C≡C is the shortest (1.28 Å) and that of C-C is the longest (1.55 Å) under the same system [46]. Therefore, by comparing the bond lengths, we find that qhp-C_{60} has two different carbon networks with sp^2 and sp^3 hybridizations. This may lead to qhp-C_{60} having different properties from other carbon materials.

In the diamond crystal, the four valence electrons of each carbon atom were sp^3 hybridized to form four identical atomic orbitals, forming covalent bonds (σ bonds) with the four most adjacent carbon atoms [47]. In addition, the carbon atoms of graphene were bonded to each other in sp^2 hybridization and formed a sizable π-conjugated system. Kaciulis pointed out that π-type bonds determined the electronic properties, such as electrical conductance and optical gap, whereas the mechanical hardness is defined by the percentage of σ bonds. Therefore, the determination of the sp^2/sp^3 ratio is decisive for characterizing all carbon allotropes. The study has shown that an appropriate sp^2/sp^3 (about 1.0–1.25) ratio will strengthen the field emission properties [48]. Low-dimensional structure materials with excellent field emission have broad application prospects in the vacuum microelectronic device. It is known that carbon-based materials such as diamond, diamond-like carbon, and carbon nanotubes. According to the results of the bond length, the value of sp^2/sp^3 in the qhp-C_{60} structure is approximately 1.4, which contributes to its application in electronic devices.

3.1.2. Formation and Binding Energy

To verify the structural stability of qhp-C_{60}, the formation and binding energy of the qhp-C_{60} are calculated using the following equations.

The enthalpy of formation is defined as the energy released (or absorbed) by the system during the formation of the compound from its elementary substance. The calculation formula is

$$\Delta H = \frac{E_{tot} - 60E_{soild}}{60} \tag{1}$$

Binding energy is the energy released by an atom from forming a compound in a free state, and is calculated as:

$$\Delta E = \frac{E_{tot} - 60E_{atom}}{60} \tag{2}$$

E_{tot} is the total energy of the qhp-C_{60}, E_{atom} is the energy of each carbon atom in a free state, and E_{soild} is the energy of a single carbon atom in the graphite. For stable structures, both the binding energy and the enthalpy of formation are negative. Generally, the smaller the value is, the more stable the system is. As shown in Table 1, the results show that the formation energy of graphene (0.05 eV/atom), diamond (0.27 eV/atom), and qhp-C_{60} (0.45 eV/atom) is greater than zero, indicating that graphite is the most stable of the four carbon materials, and the conversion of graphite to other three carbon materials is a heat-absorbing process. The binding energy of qhp-C_{60} is -8.75 eV/atom, which is close to that of graphite (-9.20 eV/atom), graphene (-9.15 eV/atom) and diamond (-8.93 eV/atom), respectively, indicating that qhp-C_{60} has excellent structural stability.

3.2. Mechanical Stability

3.2.1. Elasticity Constants

Elastic constants characterize the amount of material elasticity and reflect the ability of a crystal to resist elastic deformation. The energy–strain method is used to find the elastic constants [49]. Elastic constants of diamond are first calculated to verify the feasibility of the method. The elastic constants, bulk modulus, and shear modulus are shown in Table 2 and compared with the values in the literature. The results show that the elastic constants of the diamond obtained by the energy–strain method are consistent with the results reported in the literature, so the calculation method is available.

Table 2. Elastic constants, bulk modulus, shear modulus, Young's modulus, and Poisson's ratio of the four carbon materials.

Compound	C_{11}	C_{22}	C_{33}	C_{44}	C_{66}	C_{12}	B	G	E	v	B/G	Ref.
	GPa [a], N/m [b]									Dimensionless		
Graphite	1093.56		33.23	4.30	428.01	212.78	161.99	115.46	279.89	0.21	1.40	Present
	1211.30		36.79	4.18	468.00	275.50						[50]
Graphene	366.90	366.80			145.95	66.60	216.72	148.04	361.75	0.20	1.46	Present
	372.00					47.00						[51]
Diamond	1050.73			559.93		126.62	434.66	518.49	1112.94	0.07	0.84	Present
	1076.40			577.40		125.20						[52]
qhp-C_{60}	140.20	192.62			63.54	23.91	93.95	66.88	188.54$_{(max)}$	0.19$_{(max)}$	1.41	Present
	137.30	185.80			62.00	20.02						[53]

[a] is the unit of elastic modulus of graphite and diamond. [b] is the unit of elastic modulus of graphene and qhp-C_{60}.

As shown in Table 2, It is worth noting that our calculation results are consistent with Zhao's [53]. For two-dimensional materials, we assess their mechanical stability by the Born–Huang criterion. The two-dimensional materials need to satisfy $C_{11} > 0$, $C_{11}C_{22} - C_{12}^2 > 0$, and $C_{66} > 0$ [54], where C_{ij} is the elastic constants. C_{11} and C_{22} are the ability of the crystal to resist axial strain along the [100] and [010], respectively. C_{66} is the ability to resist shear strain on the (001), and C_{12} is the modulus along the [110] that resists shear deformation on the (110). As the results in Table 2 show, the elastic parameters of qhp-C_{60} are $C_{11} = 140.20$ N/m, $C_{22} = 192.62$ N/m, $C_{12} = 23.91$ N/m, and $C_{66} = 63.54$ N/m, respectively, which obviously satisfy the Born–Huang criterion for two-dimensional materials. Thus, qhp-C_{60} has good mechanical stability. Table 2 also shows the bulk modulus, shear modulus, and Poisson's ratio of the four carbon materials. The results show that qhp-C_{60} has the lowest bulk modulus, shear modulus, Young's modulus, and Poisson's ratio.

3.2.2. Ductility

The ductility of a crystalline could be predicted via the Pugh ratio, which is the ratio between the bulk and the shear modulus, B/G [55,56]. Pugh ratio is used empirically to predict brittle or ductile behavior of materials. In general, ductility is positively correlated with the B/G value. A larger value implies a more ductile behavior under mechanical loading. The B/G and v of the four carbon materials are compared in Figure 2. Diamond has great hardness and brittleness, so it has smaller B/G and v than other three carbon materials. The B/G and v of qhp-C_{60} are very close to those of graphite and graphene, which shows that qhp-C_{60} has similar ductility with them.
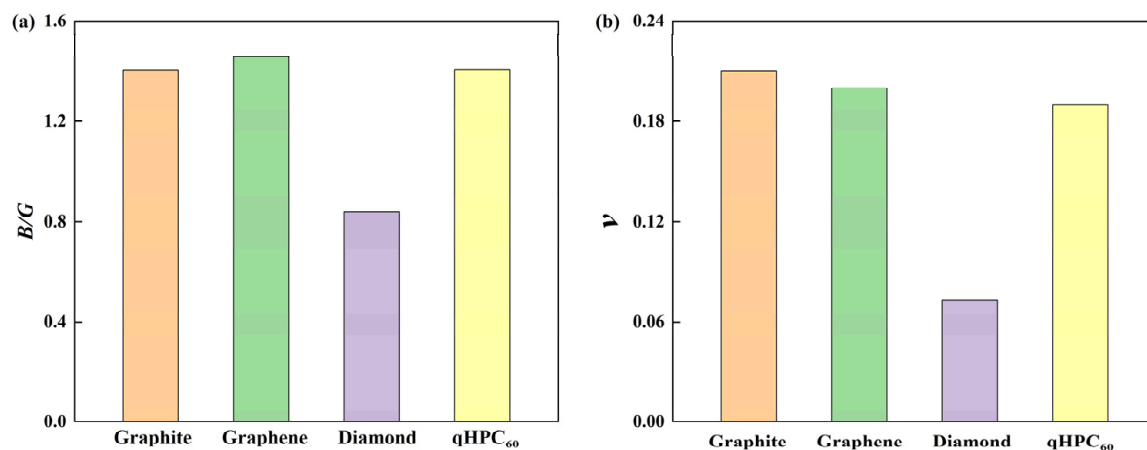
Figure 2. B/G (**a**) and Poisson's ratio (**b**) for the four carbon materials.

3.2.3. Hardness

Hardness is a crucial mechanical parameter in the mechanical properties of materials [57]. There are many empirical models for calculating the hardness (H_v) of materials. The selection of a suitable hardness model is determined based on the chemical bonding state of the material. Chen proposed a simple prediction model based on the elastic modulus of the material [58]:

$$H_{\text{chen}} = (k^2 G)^{0.585} - 3 \tag{3}$$

where k is the Pratt's modulus ratio, $k = G/B$.

An improved model based on the above model was proposed by Tian, as shown in the following equation [59]:

$$H_{\text{tian}} = 0.92 k^{1.137} G^{0.708} \tag{4}$$

Jiang explained that Young's modulus (E) could be calculated using $E = 15.76 H_{\text{jiang}}$ [60]. In addition, we use two other formulas to calculate hardness.

$$H_{\text{E}} = 0.0608 E \tag{5}$$

$$H_{\text{G}} = 0.1769 G - 2.899 \tag{6}$$

As shown in Table 3, the qhp-C$_{60}$ has the lowest hardness compared to other carbon materials.

Table 3. The hardness of the four carbon materials.

Compound	H_{chen}	H_{tian}	H_{jiang}	H_{E}	H_{G}
	GPa [a], N/m [b]				
Graphite	18.66	18.07	17.76	17.02	17.53
Graphene	20.82	20.52	22.95	21.99	23.29
Diamond	92.24	93.97	70.62	67.67	88.82
qhp-C$_{60}$	12.69	12.24	11.96	11.46	8.93

[a] is the unit of elastic modulus of graphite and diamond. [b] is the unit of elastic modulus of graphene and qhp-C$_{60}$.

3.2.4. Anisotropy of the Material

The study of mechanical properties can bring a new understanding of the application of the material. On this basis, mechanical anisotropy is also crucial to the practical use of the material, and the generation of microcracks is closely related to anisotropy [61]. Young's modulus (E) and Poisson's ratio (v) can be derived from the elastic constant combinations, as is shown in Figure 3. Young's modulus of the qhp-C60 increased from a minimum at 0° to a maximum at 90°. Similarly, we note that v exhibits strong anisotropic.
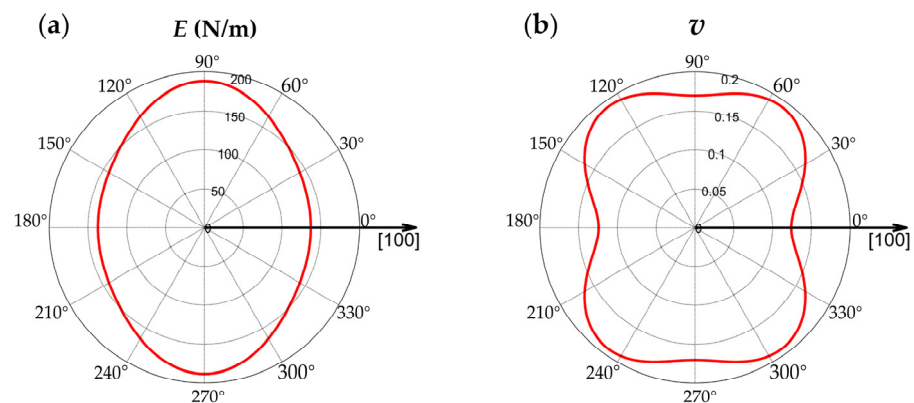

Figure 3. (**a**) Young's modulus and (**b**) Poisson's ratio of qhp-C$_{60}$.

3.3. Thermodynamic Stability

To further validate the thermodynamic stability of qhp-C_{60} via ab initio molecular dynamics (AIMD) at finite temperatures [62,63]. AIMD simulations were conducted for a $2 \times 2 \times 1$ supercell of qhp-C_{60} at the temperature of 300 K and 600 K, as shown in Figure 4a,b, which is drawn by taking a point for each 0.1 ps (100 points in total).
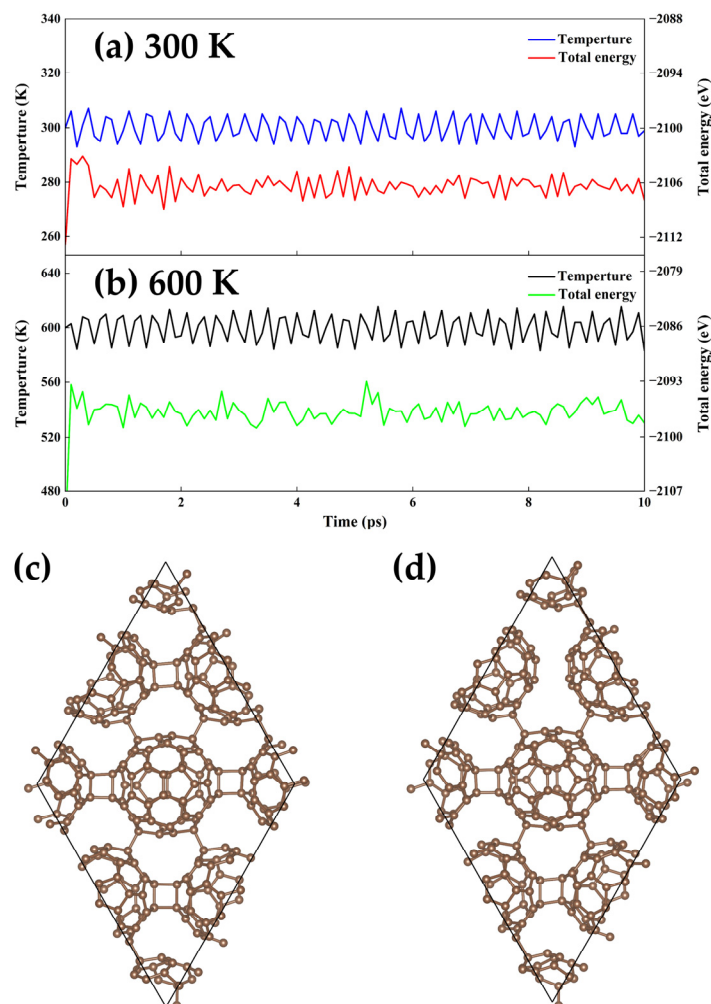

Figure 4. Total energy (left) and temperature (right) of qhp-C_{60} at (**a**) 300 K and (**b**) 600 K. The snapshot of the configuration at time of 10 ps and temperature of 300 K (**c**) and 600 K (**d**).

The AIMD results illustrated that the total energy and temperature of the system converge with fluctuations after 2 ps relaxation. The small fluctuation of the temperature and energy after convergence at 300 K reflects that the system is well equilibrated and qhp-C_{60} is thermodynamically stable at ambient conditions. The thermal dynamic equilibrium at 600 K indicates stability at high temperature.

Moreover, as shown in Figure 4c,d, although the single-layer qhp-C_{60} structure simulated by AIMD has some special bond breaks and changes, it is almost identical to its initial configuration. Our results display that qhp-C_{60} is thermodynamically stable at both 300 K and 600 K. It suggests the high-temperature applications of the qhp-C_{60} monolayer-based materials and devices.

3.4. Electronic Localization Function Analysis

In quantum chemistry, the electron localization function (ELF) is a function of the possibility of finding electrons in the neighborhood space of a given reference electron with the same spin. It is usually used to analyze the spatial localization of electron charge. In

order to further investigate the stability of qhp-C_{60} at room temperature and high temperature. The electron localization function (ELF) of qhp-C_{60} after the structural optimization at different temperatures is shown in Figure 5. Here, the ELF in the range of 0 to 1 is a space function describing the atomic bonding properties of structures, and the values of 0, 0.5, and 1 correspond to vacuum, homogeneous electron gas, and fully localized states, respectively.
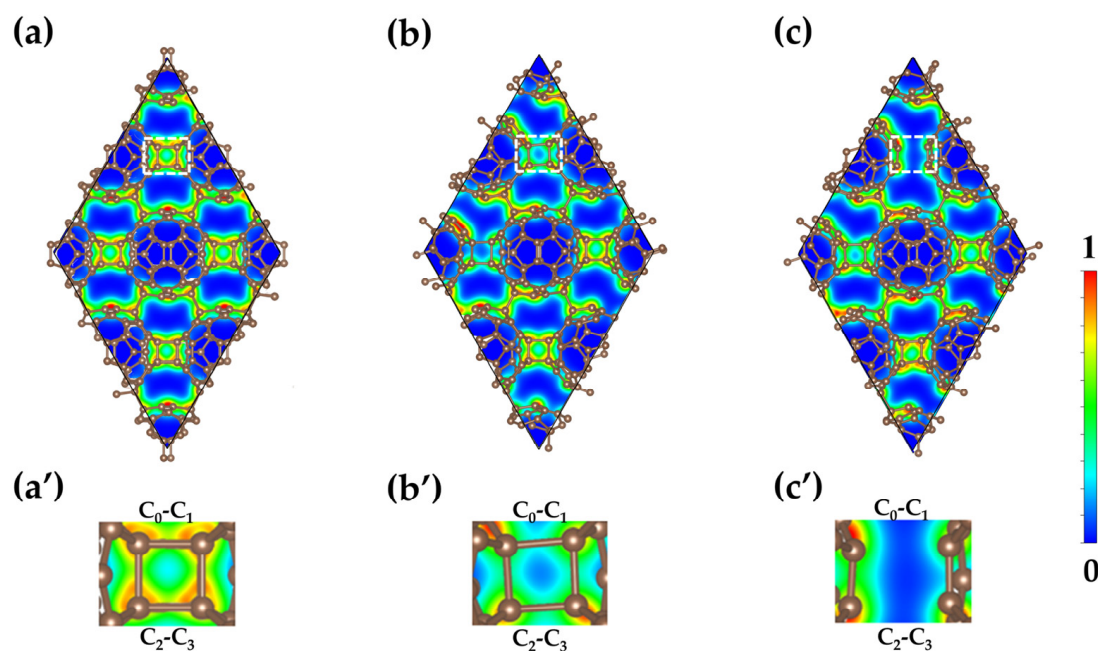
Figure 5. Electronic localization function (ELF) of qhp-C_{60} at (**a**) 0 K, (**b**) 300 K, and (**c**) 600 K. Here, (**a′**), (**b′**), and (**c′**) are, respectively, enlarged subgraphs.

As shown in Figure 5a, at a temperature of 0 K, the optimized qhp-C_{60} was found to have electron localization at the center of the bond, retaining its 2D network structure of covalent bonds, indicating that the covalent bonds between carbon atom pairs dominate. After that, as the temperature rises to room temperature, the ELF changes very little, and the charge localization of C_0-C_1 and C_2-C_3 bonds is weakened to a certain extent. At the same time, when the temperature rises to 600 K, the ELF value between C_0-C_1 and C_2-C_3 bonds becomes 0. On the other hand, the length of the C_0-C_1 bond in these three configurations is 1.61 Å, 1.68 Å, and 2.39 Å, while the C_2-C_3 bond length is 1.61 Å, 1.64 Å, and 2.51 Å, respectively. As the temperature increases, the distance between the C atom and the C atom becomes larger, the bond energy is smaller, and the bond strength also decreases, so the longer the bond, the easier it is to break. It means that the bond is broken at 600 K. However, the structure of qhp-C_{60} basically remains the original structure.

3.5. COHP and ICOHP Analysis

COHP analysis can describe the bonding characteristics between atoms and adjacent atoms, as shown in Figure 6. In general, the positive value of −COHP indicates the bond interaction, and the negative value indicates the anti-bond interaction. As the temperature increases, the interaction of carbon–carbon bonds has been decreasing and is more pronounced at 600 K.
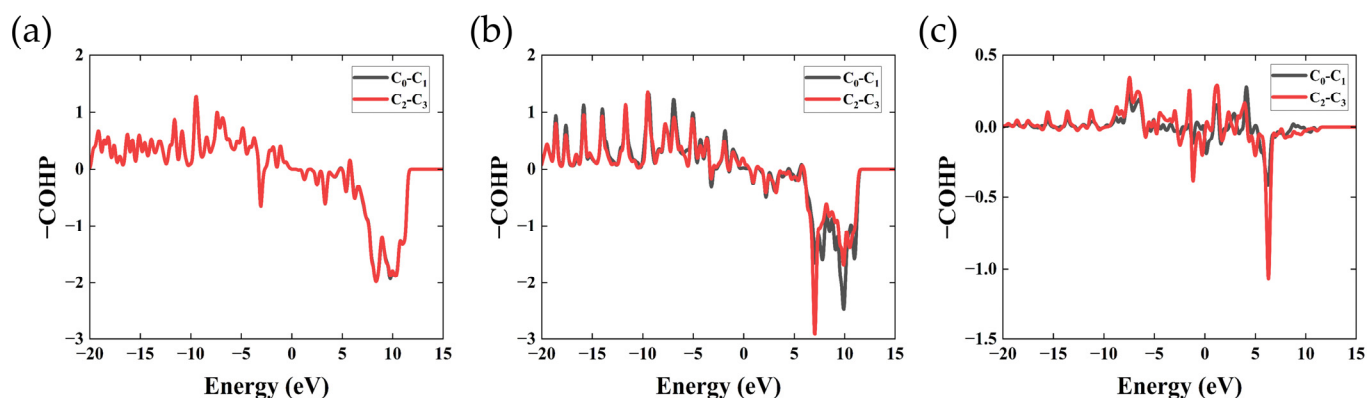
Figure 6. COHP analysis of C_0-C_1 and C_2-C_3 bonds of at (**a**) 0 K, (**b**) 300 K, and (**c**) 600 K.

The ICOHP analysis of orbital bonding strength under the configuration at a time of 10 ps and a temperature of 0 K, 300 K, and 600 K is shown in Figure 7. The integral of crystal orbital Hamilton populations (ICOHP) is obtained by integrating the Hamiltonian population below the Fermi level and can be used to measure the strength of covalent bonds in crystals. As a valuable measure of the covalent bond strength, the lower the value, the stronger the chemical bond, and vice versa [64,65]. As shown, we found that the bond lengths of C_0-C_1 and C_2-C_3 bonds increased slightly from 0 K to 300 K, and the ICOHP value also increased slightly. Therefore, the bond strength did not change much at room temperature. At this time, no bond breakage and structural changes occurred. As the temperature increases from 300 K to 600 K, the bond length and ICOHP increase dramatically. C_0-C_1 and C_2-C_3 are broken. Our first-principles study is self-consistent, which is the same as the ELF analysis.
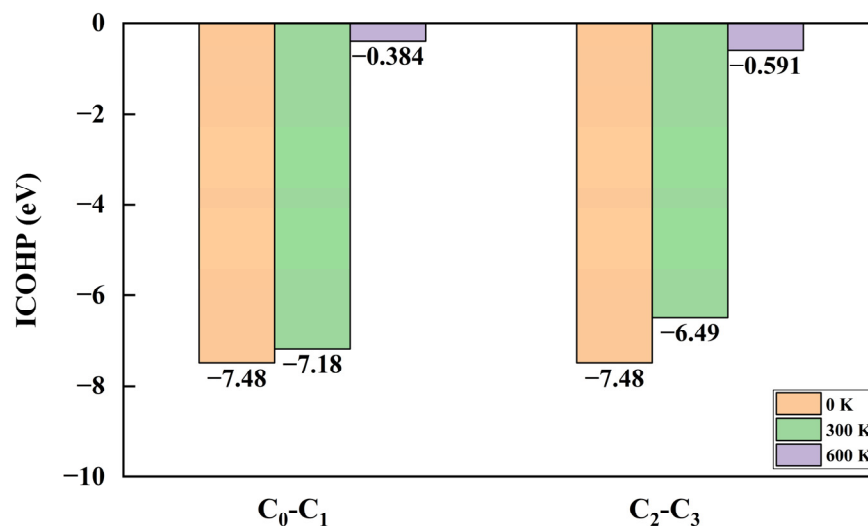

Figure 7. The ICOHP value of C_0-C_1 and C_2-C_3 bonds of at 0 K, 300 K, and 600 K.

3.6. DOS Analysis

In order to better understand the differences in orbital contributions at different temperatures. We study the projected density of states (DOS) at different temperatures. The results are shown in Figure 8. The lower valence band below the Fermi level and the above part of the conduction band are mainly contributed by the s-orbital. The outermost electron valence layer of the p-orbital is more concentrated at the Fermi level and is also the main contributor to the bonding. The contributions of the three p-orbit components (p_x, p_y, p_z) are almost the same.
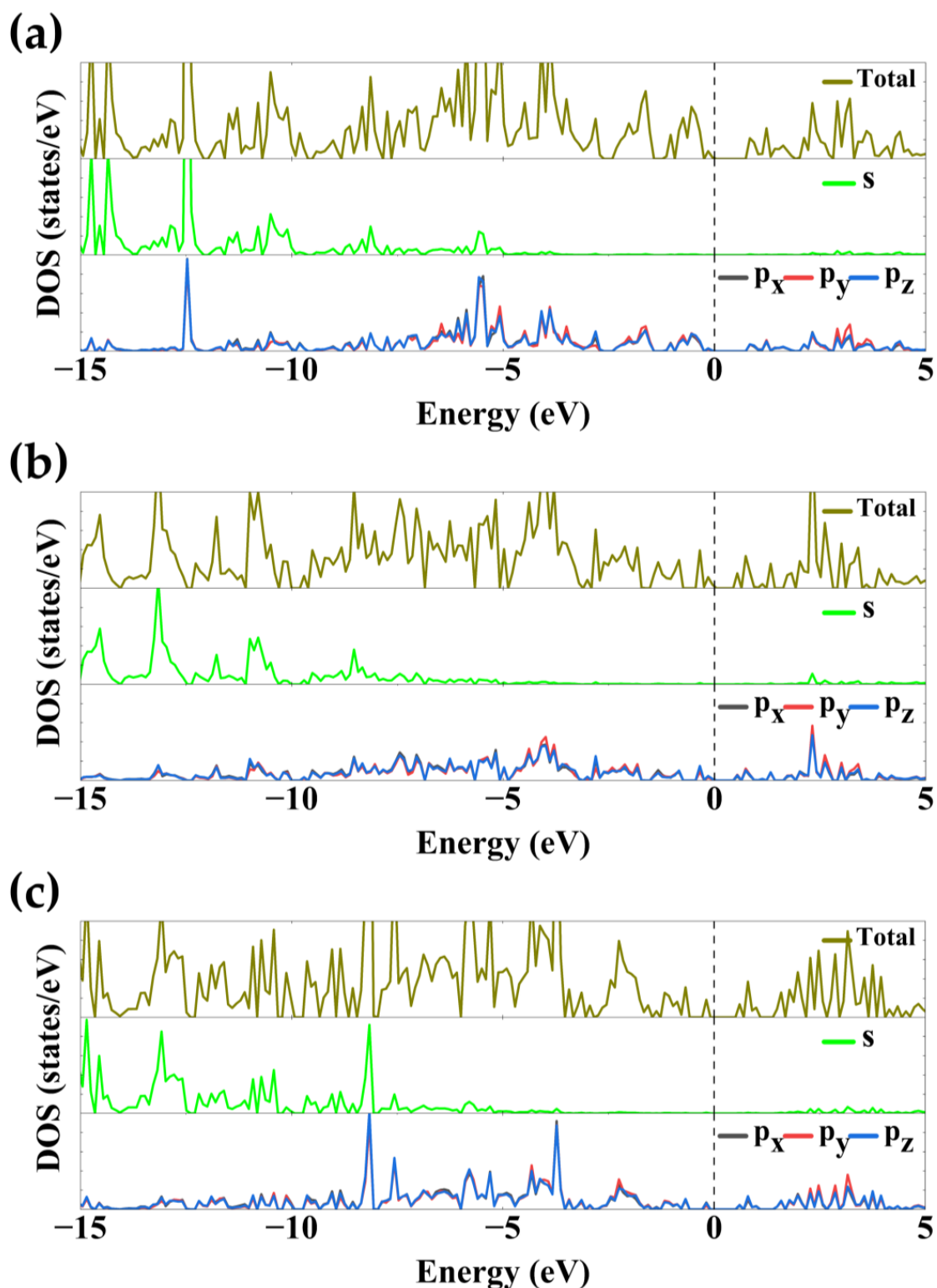
Figure 8. TDOS and PDOS of qhp-C$_{60}$ at (**a**) 0 K, (**b**) 300 K, and (**c**) 600 K.

Furthermore, we can see that qhp-C$_{60}$ has a small bandgap, and its value is approximately 0.7 eV. It is well known that the standard DFT exchange-correlation function greatly underestimates the band gap. For insulators, this is due to the discontinuous existence of energy to electron derivatives. The difference between the calculated and the experimental band gap can reach 0.5 eV [66]. The experimental and calculated values of the band gap of qhp-C$_{60}$ are 1.6 eV and 1.2 eV. Based on these facts, the calculated band gap of qhp-C$_{60}$

(0.7 eV) is in good agreement with their results. It is worth noting that the band gap values at 300 K and 600 K are 0.4 eV and 0.5 eV, respectively, with a slight decrease, indicating that the temperature rise does not seriously affect the band gap of the structure. The phenomenon provides guidance for the preparation of devices serving at high-temperature conditions.

4. Conclusions

We have investigated the stability, bonding characteristics, and mechanical properties of qhp-C_{60} by means of first-principles calculation. The formation and binding energy are calculated to verify the structural stability of qhp-C_{60}. The Born–Huang criterion is satisfied and qhp-C_{60} has good mechanical stability. The thermodynamics stability is further ensured via ab initio molecular dynamics (AIMD) at 300 K and 600 K. The analysis result of the bond length demonstrates the coexistence of two different carbon networks with sp^2 and sp^3 hybridization in qhp-C_{60}. The value of sp^2/sp^3 is approximately 1.4, implying that it can be helpful in electronic devices. Both Pugh ratio and Poisson's ratio show that qhp-C_{60} has approximate mechanical properties with graphite and graphene. In addition, qhp-C_{60} has the lowest hardness, and the values of Young's modulus and Poisson's ratio in different directions show that the material has pronounced anisotropy. The results of ELF analysis show that the bond breaks when the temperature rises to 600 K, which is also verified by COHP analysis, but the structure at this temperature still maintains the basic initial structure. The analysis of the electronic density of states shows that the contribution of the orbital does not change with the increase in temperature, but the band gap decreases.

Data Availability Statement: Data available on reasonable request.

Conflicts of Interest: The authors declare no conflict of interest.

References

1. Wu, J.; Pisula, W.; Muellen, K. Graphenes as Potential Material for Electronics. *ChemInform* **2007**, *107*, 718–747. [CrossRef]
2. Geim, A.K. Graphene: Status and Prospects. *Science* **2009**, *324*, 1530–1534. [CrossRef]
3. Ren, S.; Rong, P.; Yu, Q. Preparations, properties and applications of graphene in functional devices: A concise review. *Ceram. Int.* **2018**, *44*, 11940–11955. [CrossRef]
4. Li, X.; Cai, W.; An, J.; Kim, S.; Nah, J.; Yang, D.; Piner, R.; Velamakanni, A.; Jung, I.; Tutuc, E.; et al. Large-Area Synthesis of High-Quality and Uniform Graphene Films on Copper Foils. *Science* **2009**, *324*, 1312–1314. [CrossRef] [PubMed]
5. Chen, J.; Wen, Y.; Guo, Y.; Wu, B.; Huang, L.; Xue, Y.; Geng, D.; Wang, D.; Yu, G.; Liu, Y. Oxygen-Aided Synthesis of Polycrystalline Graphene on Silicon Dioxide Substrates. *J. Am. Chem. Soc.* **2011**, *133*, 17548–17551. [CrossRef]
6. Liu, H.; Liu, Y.; Zhu, D. Chemical doping of graphene. *J. Mater. Chem.* **2011**, *21*, 3335–3345. [CrossRef]
7. Li, X.; Zhu, Y.; Cai, W.; Borysiak, M.; Han, B.; Chen, D.; Piner, R.D.; Colombo, L.; Ruoff, R.S. Transfer of large-area graphene films for high-performance transparent conductive electrodes. *Nano Lett.* **2009**, *9*, 4359–4363. [CrossRef]
8. Bae, S.; Kim, H.; Lee, Y.; Xu, X.; Park, J.; Zheng, Y.; Balakrishnan, J.; Lei, T.; Ri Kim, H.; Song, Y.I.; et al. Roll-to-roll production of 30-inch graphene films for transparent electrodes. *Nat. Nanotechnol.* **2010**, *5*, 574–578. [CrossRef]
9. Zhu, Y.; Murali, S.; Cai, W.; Li, X.; Suk, J.W.; Potts, J.R.; Ruoff, R.S. Graphene and Graphene Oxide: Synthesis, Properties, and Applications. *Adv. Mater.* **2010**, *22*, 3906–3924. [CrossRef]

10. Wang, H.; Cui, L.F.; Yang, Y.; Sanchez, C.H.; Robinson, J.T.; Liang, Y.; Cui, Y.; Dai, H. Mn3O4-graphene hybrid as a high-capacity anode material for lithium ion batteries. *J. Am. Chem. Soc.* **2010**, *132*, 13978–13980. [CrossRef]

11. Zhu, Y.; Murali, S.; Stoller, M.D.; Ganesh, K.J.; Cai, W.; Ferreira, P.J.; Pirkle, A.; Wallace, R.M.; Cychosz, K.A.; Thommes, M.; et al. Carbon-based supercapacitors produced by activation of graphene. *Science* **2011**, *332*, 1537–1541. [CrossRef] [PubMed]

12. Lee, J.K.; Smith, K.B.; Hayner, C.M.; Kung, H.H. Silicon nanoparticles–graphene paper composites for Li ion battery anodes. *Chem. Commun.* **2010**, *46*, 2025–2027. [CrossRef]

13. Novoselov, K.S.; Geim, A.K.; Morozov, S.V.; Jiang, D.; Zhang, Y.; Dubonos, S.V.; Grigorieva, I.V.; Firsov, A.A. Electric Field Effect in Atomically Thin Carbon Films. *Science* **2004**, *306*, 666–669. [CrossRef]

14. Frindt, R.F. Single Crystals of MoS2 Several Molecular Layers Thick. *J. Appl. Phys.* **1966**, *37*, 1928–1929. [CrossRef]

15. Joensen, P.; Frindt, R.F.; Morrison, S.R. Single-layer MoS2. *Mater. Res. Bull.* **1986**, *21*, 457–461. [CrossRef]

16. Novoselov, K.; Jiang, D.; Schedin, F.; Booth, T.; Khotkevich, V.V.; Morozov, S.; Geim, A. Two Dimentional Atomic Crystals. *Proc. Natl. Acad. Sci. USA* **2005**, *102*, 10451. [CrossRef]

17. Wang, R.; Peng, D.; Hu, J.; Zong, L.; Chen, X. Orientational ordering and electron-phonon interaction in K_3C_{60} superconductor. *Carbon* **2022**, *195*, 1–8. [CrossRef]

18. Zong, L.; Wang, R.; Peng, D.; Chen, X. Superconductivity in Nonstoichiometric Rubidium-Doped C_{60}. *J. Phys. Chem. C* **2022**, *126*, 2912–2919. [CrossRef]

19. Wang, R.; Peng, D.; Zong, L.; Chen, L.; Chen, X. Variation of the critical temperature with the lattice parameter in K_3C_{60}. *Carbon* **2022**, *199*, 181–188. [CrossRef]

20. Wang, R.; Peng, D.; Zong, L.; Zhu, Z.; Chen, X. Full set of superconducting parameters of K_3C_{60}. *Carbon* **2023**, *202*, 325–335. [CrossRef]

21. Hou, L.; Cui, X.; Guan, B.; Wang, S.; Li, R.; Liu, Y.; Zhu, D.; Zheng, J. Synthesis of a monolayer fullerene network. *Nature* **2022**, *606*, 507–510. [CrossRef] [PubMed]

22. Dungey, K.E.; Curtis, M.D.; Hahn, J.E.P. Structural characterization and thermal stability of MoS2 intercalation compounds. *Chem. Mater.* **1998**, *10*, 2152–2161. [CrossRef]

23. Ouyang, T.; Chen, Y.; Xie, Y.; Yang, K.; Bao, Z.; Zhong, J. Thermal transport in hexagonal boron nitride nanoribbons. *Nanotechnology* **2010**, *21*, 245701. [CrossRef]

24. Tang, S.; Lan, H.; Duan, L.; Jin, J.; Li, J.; Liu, Z.; Wang, G. Co-Precipitation Behavior in Ferrite Region During Isothermal Process in Ti-Mo-Cu Microalloyed Steel. *Acta Metall. Sin.* **2022**, *58*, 355–364. [CrossRef]

25. Radisavljevic, B.; Kis, A. Mobility engineering and a metal-insulator transition in monolayer MoS_2. *Nat. Mater.* **2013**, *12*, 815–820. [CrossRef]

26. Kiriya, D.; Tosun, M.; Zhao, P.; Kang, J.S.; Javey, A. Air-Stable Surface Charge Transfer Doping of MoS2 by Benzyl Viologen. *J. Am. Chem. Soc.* **2014**, *136*, 7853–7856. [CrossRef]

27. Yang, S.; Park, S.; Jang, S.; Kim, H.; Kwon, J. Electrical stability of multilayer MoS2 field-effect transistor under negative bias stress at various temperatures. *Phys. Status Solidi Rapid Res. Lett.* **2014**, *8*, 714–718. [CrossRef]

28. Fan, X.; Zheng, W.T.; Kuo, J.L.; Singh, D.J. Structural stability of single-layer MoS2 under large strain. *J. Phys. Condens. Matter* **2015**, *27*, 105401. [CrossRef]

29. Sen, D.; Das, B.K.; Saha, S.; Roy, R.; Mitra, A.; Chattopadhyay, K.K. sp(3) bonded 2-dimensional allotrope of carbon: A first-principles prediction. *Carbon* **2019**, *146*, 430–437. [CrossRef]

30. Li, L.H.; Cervenka, J.; Watanabe, K.; Taniguchi, T.; Chen, Y. Strong oxidation resistance of atomically thin boron nitride nanosheets. *ACS Nano* **2014**, *8*, 1457–1462. [CrossRef]

31. Wen, B.; Takami, S.; Kawazoe, Y.; Adschiri, T. Pressure-dependent mechanical stability of simple cubic carbon. *Phys. B Condens. Matter* **2011**, *406*, 2654–2657. [CrossRef]

32. Lu, Y.; Zhu, X.; Wang, M. Theoretical investigations of a new two-dimensional carbon allotrope: hP-C23-2D. *Comput. Mater. Sci.* **2019**, *167*, 8–12. [CrossRef]

33. He, C.; Sun, L.; Zhang, C.; Zhong, J. Two viable three-dimensional carbon semiconductors with an entirely sp2 configuration. *Phys. Chem. Chem. Phys.* **2013**, *15*, 680–684. [CrossRef] [PubMed]

34. Luo, Y.; Ren, C.; Xu, Y.; Yu, J.; Wang, S.; Sun, M. A first principles investigation on the structural, mechanical, electronic, and catalytic properties of biphenylene. *Sci. Rep.* **2021**, *11*, 19008. [CrossRef] [PubMed]

35. Mortazavi, B.; Zhuang, X. Low and Anisotropic Tensile Strength and Thermal Conductivity in the Single-Layer Fullerene Network Predicted by Machine-Learning Interatomic Potentials. *Coatings* **2022**, *12*, 1171. [CrossRef]

36. Mei, H.; Zhong, Y.; He, D.; Du, X.; Li, C.; Cheng, N. Predicting the structural, elastic and electronic properties of new two-dimensional carbon and silicon monolayers. *Results Phys.* **2020**, *16*, 102826. [CrossRef]

37. Alborznia, H.; Naseri, M.; Fatahi, N. Pressure effects on the optical and electronic aspects of T-Carbon: A first principles calculation. *Optik* **2019**, *180*, 125–133. [CrossRef]

38. Wang, Y.; Zeng, Q.; Du, X.; Gao, Y.; Yin, B. The structural, mechanical and electronic properties of novel superhard carbon allotropes: Ab initio study. *Mater. Today Commun.* **2021**, *29*, 102980. [CrossRef]

39. Kresse, G.; Furthmüller, J. Efficient Iterative Schemes for Ab Initio Total-Energy Calculations Using a Plane-Wave Basis Set. *Phys. Rev. B* **1996**, *54*, 11169. [CrossRef]

40. Blöchl, P.E. Projector augmented-wave method. *Phys. Rev. B* **1994**, *50*, 17953–17979. [CrossRef]

41. Burke, K.; Ernzerhof, M.; Perdew, J.P. Generalized Gradient Approximation Made Simple. *Phys. Rev. Lett.* **1996**, *77*, 3865–3868. [CrossRef]
42. Tang, S.; Li, L.-X.; Peng, Q.; Yan, H.-L.; Cai, M.-H.; Li, J.-P.; Liu, Z.-Y.; Wang, G.-D. First-principles insights into hydrogen trapping in interstitial-vacancy complexes in vanadium carbide. *Phys. Chem. Chem. Phys.* **2022**, *24*, 20400–20408. [CrossRef] [PubMed]
43. Occelli, F.; Loubeyre, P.; LeToullec, R. Properties of diamond under hydrostatic pressures up to 140 GPa. *Nat. Mater.* **2003**, *2*, 151–154. [CrossRef] [PubMed]
44. Gao, Y.; Feng, X.; Gong, B.; Zhong, C.; Yang, S.A.; Liu, K.; Lu, Z. Theoretical design of all-carbon networks with intrinsic magnetism. *Carbon* **2021**, *177*, 11–18. [CrossRef]
45. Wang, J.; Mizuseki, H.; Chen, C.; Li, Z. Computational discovery of a new rhombohedral diamond phase. *Phys. Rev. B* **2018**, *98*, 094107. [CrossRef]
46. Vejpravová, J. Mixed sp^2–sp^3 Nanocarbon Materials: A Status Quo Review. *Nanomaterials* **2021**, *11*, 2469. [CrossRef]
47. Popov, A.A.; Yang, S.; Dunsch, L. Endohedral fullerenes. *Chem. Rev.* **2013**, *113*, 5989–6113. [CrossRef]
48. Wang, Q.; Jiang, J. An overview on structure and field emission properties of carbon nitride films. *J. Nanomater.* **2014**, *2014*, 10. [CrossRef]
49. Hu, Q.M.; Yang, R. Mechanical properties of structural materials from first-principles. *Curr. Opin. Solid State Mater. Sci.* **2006**, *10*, 19–25. [CrossRef]
50. Michel, K.H.; Verberck, B. Theory of the elastic constants of graphite and graphene. *Phys Status Solidi B* **2008**, *245*, 2177–2180. [CrossRef]
51. Sun, Y.W.; Papageorgiou, D.G.; Humphreys, C.J.; Dunstan, D.J.; Puech, P.; Proctor, J.E.; Bousige, C.; Machon, D.; San-Miguel, A. Mechanical properties of graphene. *Appl. Phys. Rev.* **2021**, *8*, 021310. [CrossRef]
52. Ramdas, A.K.; Grimsditch, M.H. Brillouin scattering in diamond. *Phys. Rev. B* **1975**, *11*, 3139–3148. [CrossRef]
53. Zhao, S.; Zhang, X.; Ni, Y.; Peng, Q.; Wei, Y. Anisotropic mechanical response of a 2D covalently bound fullerene lattice. *Carbon* **2022**, *202*, 118–124. [CrossRef]
54. Fang, W.; Li, P.; Yuan, J.; Xue, K.; Wang, J. Nb2SiTe4 and Nb2GeTe4: Unexplored 2D Ternary Layered Tellurides with High Stability, Narrow Band Gap and High Electron Mobility. *J. Electron. Mater.* **2020**, *49*, 959–968. [CrossRef]
55. Pugh, S.F. XCII. Relations between the elastic moduli and the plastic properties of polycrystalline pure metals. *Lond. Edinb. Dublin Philos. Mag. J. Sci.* **1954**, *45*, 823–843. [CrossRef]
56. Chen, H.; Cao, Y.; Liu, K.; Tao, X.; Zhou, Y.; Ouyang, Y.; Gao, F.; Du, Y.; Peng, Q. Stability and physical properties tuning via interstitials chemical engineering of Zr5Sn3: A first-principles study. *J. Mater. Sci.* **2019**, *54*, 10284–10296. [CrossRef]
57. Mannepalli, S.; Mangalampalli, K. Indentation Plasticity and Fracture Studies of Organic Crystals. *Crystals* **2017**, *7*, 324. [CrossRef]
58. Chen, X.; Niu, H.; Li, D.; Li, Y. Modeling hardness of polycrystalline materials and bulk metallic glasses. *Intermetallics* **2011**, *19*, 1275–1281. [CrossRef]
59. Tian, Y.; Xu, B.; Zhao, Z. Microscopic theory of hardness and design of novel superhard crystals. *Int. J. Refract. Hard Met.* **2012**, *33*, 93–106. [CrossRef]
60. Jiang, X.; Zhao, J.; Aimin, W.; Bai, Y.; Jiang, X. Mechanical and electronic properties of B-12-based ternary crystals of orthorhombic phase. *J. Phys. Condens. Matter* **2010**, *22*, 315503. [CrossRef]
61. Sayers, C.M.; Kachanov, M. Microcrack-induced elastic wave anisotropy of brittle rocks. *J. Geophys. Res. Solid Earth* **1995**, *100*, 4149–4156. [CrossRef]
62. Gorenstein, M.I.; Zozulya, O.S.; Begun, V.V. Fluctuations in the canonical ensemble. *Phys. Rev. C* **2005**, *72*, 014902. [CrossRef]
63. Singh, N.J.; Yi, H.B.; Min, S.K.; Park, M.; Kim, K.S. Dissolution nature of cesium fluoride by water molecules. *J. Phys. Chem. B* **2006**, *110*, 3808–3815. [CrossRef] [PubMed]
64. Dronskowski, R.; Bloechl, P.E. Crystal orbital Hamilton populations (COHP): Energy-resolved visualization of chemical bonding in solids based on density-functional calculations. *J. Phys. Chem. A* **1993**, *97*, 8617–8624. [CrossRef]
65. Gu, X.J.; Poon, S.J.; Shiflet, G.J.; Widom, M. Ductility improvement of amorphous steels: Roles of shear modulus and electronic structure. *Acta Mater.* **2008**, *56*, 88–94. [CrossRef]
66. Xiao, H.; Tahir-Kheli, J.; Goddard, W.A.I. Accurate Band Gaps for Semiconductors from Density Functional Theory. *J. Phys. Chem. Lett.* **2011**, *2*, 212–217. [CrossRef]